Supplementary Material of "Tensor Ring Decomposition Guided Dictionary Learning for OCT Images Denoising"

Parisa Ghaderi Daneshmand[1], Hossein Rabbani[*,1], Senior Member, IEEE

[1]Medical Image & Signal Processing Research Center, School of Advanced Technologies in Medicine, Isfahan University of Medical Sciences, Isfahan, Iran

I. Overview

This supplementary material includes the following sections. Section II shows the algorithm of the proposed TRGDL model for OCT image denoising. In Section III, we provided the quantitative and qualitative results for denoising OCT images of dataset-3. Section IV presents the effect of suggested TRGDL model to the layer segmentation. Finally, we investigate the computational complexity of our proposed TRGDL model in Section V.

[*]Corresponding author

II. Algorithm of the proposed TRGDL model for OCT image denoising

The suggested TRGDL model for OCT denoising is shown in Algorithm 1.

Algorithm1 : The suggested TRGDL for OCT image denoising

Input: Noisy OCT tensor $\mathcal{Y}$

Initialization:

1) Tune the parameters such as TR rank, patch size, redundancy ratios, regularization parameters, iteration number, Proximal parameter, etc.

2) Initialize $\boldsymbol{D_S}$ and $\boldsymbol{D_T}$ randomly and then normalize each column of these dictionaries.

For t =1, 2…, t_{max} **do**

$\mathcal{Y}^{(t)} = \mathcal{Y}^{(t-1)} + \delta(\mathcal{Y} - \mathcal{Y}^{(t-1)})$

while not converged **do**

3) Construct OCT group tensors ($\mathcal{Y}^k$, k=1, 2,…..,K)

4) Solving Eq. (17) through proximal alternating minimization (PAM) [1] and alternative direction method of multipliers (ADMM) [2];

For k = 1, 2, … K **do**

Update $\mathcal{L}^k$ via Eq. (18)

Update $\mathcal{A}^k$ by Eq. (23)

Update $\mathcal{Q}^k$ via Eq. (25)

Update $\mathcal{M}^k$ by Eq. (28)

End

Update $\boldsymbol{D_S}$ via Eq. (30)

Update $\boldsymbol{D_T}$ by Eq. (32)

End whlie

5) Reconstruct OCT group tensors via $\hat{\mathcal{Y}}^k = \mathcal{A}^k \times_1 \mathbf{D}_S \times_2 \mathbf{D}_T$ (k=1, 2,…..,K)

6) Aggregate all $\hat{\mathcal{Y}}^k$ to construct the denoised image

End

7) Output: Denoised OCT tensor $\hat{\mathcal{Y}}$

III. Results for OCT Images Denoising of Dataset-3

This section provides qualitative and quantitative results for the noise suppression experiment of dataset-3. Fig.S1 and Table. S1 show results of all compared techniques. As Fig.S1 shows, the proposed TRGDL has the most pleasing performance in maintaining layer structures and reducing the noise. Moreover, this method outperforms other rival methods in terms of CNR, and MSR.

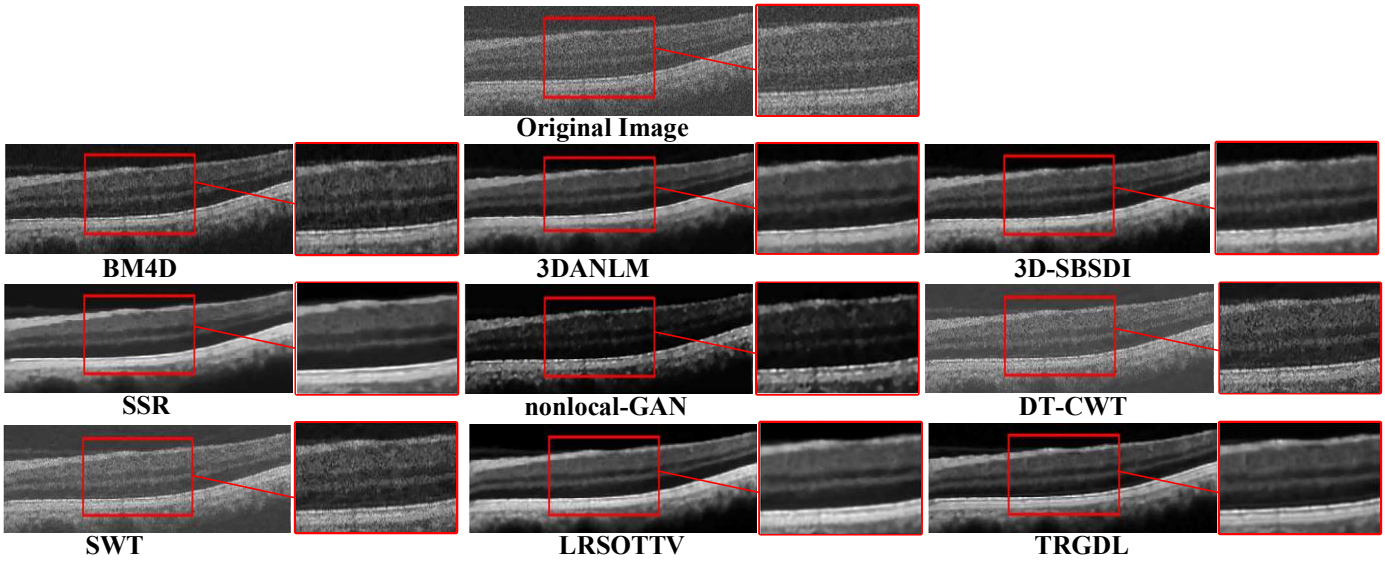

Fig.S1 One retinal OCT image in the dataset-3 and their denoising results utilizing the BM4D [3], 3DANLM [4], 3D-SBSDI [5], SSR [6], nonlocal-GAN [7], DT-CWT [8], SWT [8], LRSOTTV [9], and the suggested TRGDL approach.

Table.S1 Mean & Standard deviation of the MSR and CNR results for denoising dataset-3 by various approaches. Best results are bolded. Where $p < 0.05$, the measures for each test approach are statistically significant and characterized by a* symbol.

	CNR		MSR	
	Mean± SD	**P-value**	**Mean± SD**	**P-value**
Noisy	2.17±0.28	4.00E-05*	4.48±0.34	4.00E-05*
BM4D	3.63±0.77	4.00E-05*	8.09±1.32	4.00E-05*
3DANLM	4.46±1.32	1.05E-04*	12.15±3.37	4.00E-05*
3D-SBSDI	4.54±1.35	4.83E-04*	12.31±3.16	4.00E-05*
SSR	4.18±1.23	7.00E-05*	12.78±3.70	8.00E-05*
DT-CWT	3.21±0.51	4.00E-05*	6.53±0.77	4.00E-05*
SWT	3.41±0.59	4.00E-05*	7.11±0.89	4.00E-05*
nonlocal-GAN	2.71±0.82	4.00E-05*	12.48±2.99	3.34E-04*
LRSOTTV	4.56±1.39	1.54E-03*	12.89±3.76	4.00E-05*
TRGDL	**4.65**±1.45	-	**14.11**±4.14	-

IV. Effect of suggested TRGDL model to the layer segmentation

In retinal OCT images, the layers contain important information about the pathological and anatomical structures. Therefore, the segmentation of these layers is an important process in analyzing ocular disorders. Thus, it is expected that the resulting images from the denoising process not only keep the meaningful structures, but also make the segmentation outcomes more exact. To prove the usefulness of the denoised outcomes for layer segmentation, we used the retinal images of dataset-3 that are captured from normal subjects. We fed the noisy raw images and the denoised images acquired by various methods into a diffusion map-based segmentation method [10] to segment 12 different layers of OCT images. The layers include the internal limiting membrane (ILM), nerve fiber layer (NFL), ganglion cell layer (GCL), inner plexiform layer (IPL), inner nuclear layer (INL), outer plexiform layer (OPL), outer nuclear layer (ONL), Photoreceptors, inner segment of rods and cones (IS), outer segment of rods and cones (OS), retinal pigment epithelium (RPE). Then, using the borders which were manually determined by ophthalmologists, we calculated the unsigned errors of border positioning. The mean of unsigned errors for each layer of OCT images is presented in Table S2 (on noisy raw and the denoised images by various methods). The average error on all 12 layers is presented in the final column of the table.

Table.S2 Unsigned border positioning error on 12 retinal layers from dataset-3.

	ILM	NFL-GC	GCL-IPL	IPL-INL	INL-OPL	OPL-ONL	Photo receptor	IS/OS	OS-RPE	RPE/A	RPE/B	RPE/C	overall
Noisy	1.1661	2.2313	4.0728	4.8555	3.6111	3.7476	2.3134	0.9266	1.0449	0.9894	0.9966	0.9677	2.2436
BM4D	**1.1601**	2.2753	4.4445	3.3707	3.7961	3.4842	2.2131	0.8418	1.0858	0.9190	1.1398	0.9843	2.1429
3DANLM	1.2833	2.5471	4.8093	4.0061	4.2037	3.3173	2.1307	0.9039	1.1343	1.0691	1.1945	1.0904	2.3075
3D-SBSDI	1.2317	2.4557	4.2153	3.1858	3.7596	3.0711	**2.1196**	**0.8321**	1.0178	0.8667	1.1346	**0.8983**	2.0657
SSR	1.1633	2.3006	5.2130	3.3775	3.9691	3.3003	2.2548	0.9648	1.0428	0.8694	1.2529	0.9923	2.2251
DT-CWT	1.1629	2.3814	4.0217	4.0974	3.5408	3.6411	2.2335	0.8685	1.0523	1.0300	1.0004	0.9635	2.1661
SWT	1.1663	2.3605	3.8389	3.3724	3.6581	3.6405	2.2759	0.9079	1.0528	1.0151	**0.9758**	0.9559	2.1017
Nonlocal-GAN	1.2291	2.3380	4.5742	4.5690	3.9346	4.7357	2.2433	0.9034	**0.9165**	**0.6565**	1.0782	0.9920	2.3475
LRSOTTV	1.2531	2.4252	4.1858	2.2918	3.5852	**2.2913**	2.2388	0.9811	1.0046	0.9758	1.4299	1.0642	1.9772
TRGDL	1.2197	**2.2255**	**3.8251**	**1.8709**	**3.3499**	2.4142	2.1892	0.8989	1.0173	0.8355	1.1303	1.0688	**1.8371**

It can be seen that the accuracy of the border positioning in most layers is improved after employing the suggested TRGDL approach in comparison with the raw noisy data and most of techniques. The overall unsigned error in our suggested TRGDL model is 1.8371, while its value is 2.2436 for the noisy raw image, error value being higher in rival techniques.

V. Computational Complexity

In each iteration, the computational complexity of the suggested TRGDL model mainly contains two main parts. 1) Considering fixed dictionaries and solving four sub-problems including $\mathcal{L}^k$, $\mathcal{A}^k$, $\mathcal{Q}^k$, and $\mathcal{M}^k$ subproblems for each group tensor (k=1, 2… , K) . 2) Dictionary updating. In the first part, the main computational complexity lies in the solving the $\mathcal{L}^k$ sub-problem and updating $\mathcal{Z}^k$. Assuming that we have a tensor $\mathcal{Y}^k \in R^{I_1 \times I_2 \times I_3}$ where $I_1=I_2=I_3=I$, TR-rank is considered as $R_1=R_2=R_N=R$, the computational cost of updating the $\mathcal{L}^k$ is $O\left(R^6 + R^4 I^2 + R^2 I^3\right)$, and therefore the overall complexity for K group tensors is about $O\left(K(R^6 + R^4 I^2 + R^2 I^3)\right)$. In the second part, the complexity of updating $\mathbf{D}_S$ and $\mathbf{D}_T$ is $O\left(P_{total}(\omega_S pp)^2 + P_{total}(\omega_T V)^2\right)$.

Bibliography

[1] N. Parikh and S. Boyd, "Proximal algorithms," *Foundations and trends® in Optimization,* vol. 1, no. 3, pp. 127-239, 2014.

[2] S. Boyd, N. Parikh, E. Chu, B. Peleato, and J. Eckstein, "Distributed optimization and statistical learning via the alternating direction method of multipliers," *Foundations and Trends® in Machine learning,* vol. 3, no. 1, pp. 1-122, 2011.

[3] M. Maggioni, V. Katkovnik, K. Egiazarian, and A. Foi, "Nonlocal transform-domain filter for volumetric data denoising and reconstruction," *IEEE transactions on image processing,* vol. 22, no. 1, pp. 119-133, 2012.

[4] J. V. Manjón, P. Coupé, L. Martí-Bonmatí, D. L. Collins, and M. Robles, "Adaptive non-local means denoising of MR images with spatially varying noise levels," *Journal of Magnetic Resonance Imaging,* vol. 31, no. 1, pp. 192-203, 2010.

[5] L. Fang *et al.*, "Fast acquisition and reconstruction of optical coherence tomography images via sparse representation," *IEEE transactions on medical imaging,* vol. 32, no. 11, pp. 2034-2049, 2013.

[6] L. Fang, S. Li, D. Cunefare, and S. Farsiu, "Segmentation based sparse reconstruction of optical coherence tomography images," *IEEE transactions on medical imaging,* vol. 36, no. 2, pp. 407-421, 2016.

[7] A. Guo, L. Fang, M. Qi, and S. Li, "Unsupervised denoising of optical coherence tomography images with nonlocal-generative adversarial network," *IEEE Transactions on Instrumentation and Measurement,* vol. 70, pp. 1-12, 2020.

[8] P. Arun, V. P. Gopi, and P. Palanisamy, "Despeckling of OCT images using DT-CWT based fusion technique," *Optik,* vol. 263, p. 169332, 2022.

[9] P. G. Daneshmand, A. Mehridehnavi, and H. Rabbani, "Reconstruction of optical coherence tomography images using mixed low rank approximation and second order tensor based total variation method," *IEEE Transactions on Medical Imaging,* vol. 40, no. 3, pp. 865-878, 2020.

[10] R. Kafieh, H. Rabbani, M. D. Abramoff, and M. Sonka, "Intra-retinal layer segmentation of 3D optical coherence tomography using coarse grained diffusion map," *Medical image analysis,* vol. 17, no. 8, pp. 907-928, 2013.